Fermi National Accelerator Laboratory

Probing the Universe with the Lyman-alpha Forest:
I. Hydrodynamics of the Low Density IGM

Nickolay Y. Gnedin

Department of Astronomy
University of California, Berkeley, California 94720

Lam Hui

Fermi National Accelerator Laboratory
P.O. Box 500, Batavia, Illinois 60510

June 1997

Disclaimer

Distribution

Probing the Universe with the Lyman-alpha Forest:

I. Hydrodynamics of the Low Density IGM

Nickolay Y. Gnedin[*]

Department of Astronomy
University of California, Berkeley, CA 94720

Lam Hui[†]

NASA/Fermilab Astrophysics Center
Fermi National Accelerator Laboratory, Batavia, IL 60510

[*] email: gnedin@tac-1.berkeley.edu

[†] email: lhui@hydra.fnal.gov

ABSTRACT

We introduce an efficient and accurate alternative to full hydrodynamic simulations, Hydro-PM (HPM), for the study of the low column density Lyman-alpha forest ($N_{HI} \lesssim 10^{14}\,\mathrm{cm}^{-2}$). It consists of a Particle-Mesh (PM) solver, modified to compute, in addition to the gravitational potential, an effective potential due to the gas pressure. Such an effective potential can be computed from the density field because of a tight correlation between density and pressure in the low density limit ($\delta \lesssim 10$), which can be calculated for any photo-reionization history by a method outlined in Hui & Gnedin (1997). Such a correlation exists, in part, because of minimal shock-heating in the low density limit. We compare carefully the density and velocity fields as well as absorption spectra, computed using HPM versus hydrodynamic simulations, and find good agreement. We show that HPM is capable of reproducing measurable quantities, such as the column density distribution, computed from full hydrodynamic simulations, to a precision comparable to that of observations. We discuss how, by virtue of its speed and accuracy, HPM can enable us to use the Lyman-alpha forest as a cosmological probe.

We also discuss in detail the smoothing of the gas (or baryon) fluctuation relative to that of the dark matter on small scales due to finite gas pressure: (1) It is shown the conventional wisdom that the linear gas fluctuation is smoothed on the Jeans scale is incorrect for general reionization (or reheating) history; the correct linear filtering scale is in general smaller than the Jeans scale after reheating, but larger prior to it. (2) It is demonstrated further that in the mildly nonlinear regime, a PM solver, combined with suitable pre-filtering of the initial conditions, can be used to model the low density IGM. But such an approximation is shown to be less accurate than HPM, unless a non-uniform pre-filtering scheme is implemented.

Key words: cosmology: theory — intergalactic medium — quasars: absorption lines – methods: numerical – hydrodynamics

INTRODUCTION

The low density intergalactic medium, filling the enormous space between galaxies and their aggregations, offers cosmologists a unique and powerful probe of the high redshift universe ($z \sim 2 - 5$), still inaccessible for large galaxy surveys. The intergalactic medium (hereafter IGM) manifests itself observationally in the numerous weak absorption lines along a line of sight to a distant quasar, the Lyman-alpha forest. Up to date, an enormous treasury of observational data on the Lyman-alpha forest at a wide range of redshifts has been collected (see, for example, Hu et al. 1995, Lu et al. 1996, Cristiani et al. 1996, Kirkman & Tytler 1997, Kim et al. 1997 and D'Odorico et al. 1997 for most recent observational advances). Several models were proposed to explain the Lyman-alpha forest (Bahcall & Salpeter 1965; Arons 1972; Black 1981; Ostriker & Ikeuchi 1983; Ikeuchi & Ostriker 1986; Rees 1986; Ikeuchi 1986; Rees 1988; Bond, Szalay, & Silk 1988; McGill 1990; Bi, Börner & Chu 1992). However, it was only after several groups (Cen et al. 1994; Zhang, Anninos, & Norman 1995; Hernquist et al. 1996; Miralda-Escudé et al. 1996; Wadsley & Bond 1996; Zhang et al. 1997) performed cosmological hydrodynamic simulations when it became apparent that at least an appreciable fraction of the Lyman-alpha forest consists of smooth fluctuations in the IGM, which arise naturally under gravitational instability, rather than discrete absorbers, as has been believed before.

Abundance of observational data and the existence of a compelling theoretical framework (i.e. hierarchical clustering) allows one to make detailed comparisons between observations and predictions of a given cosmological model. Moreover, one might even attempt to use the observational data in a maximum-likehood type analysis to infer cosmological parameters, either in a model-independent way, or at least within a class of models. A recent example towards this direction is the use of the observed mean Lyman-alpha optical depth to put limits on the baryon content of the universe (Miralda-Escudé et al. 1996; Rauch, et al.1996; Bi & Davidsen 1997; Weinberg et al. 1997). One might contemplate going a step further to use other properties of the Lyman-alpha forest as a probe of equally interesting cosmological parameters such as the normalization and slope of the power spectrum (see, for example, Hui, Gnedin & Zhang 1997), the massive neutrino density, the epoch of reionization and so on.

However, while hydrodynamic simulations give us insights into the physical properties of the IGM as well as definite predictions for a given cosmological model (provided, numerical resolution and physical modelling are adequate), computational expense makes them impractical to use in a maximum-likehood type of analysis in which a large range of models are considered.

It is therefore important to ask whether a more efficient, and at the same time sufficiently accurate, approximate method can be developed in place of full hydrodynamic simulations.

Up to date, two different semi-analytical approximations have been used: the lognormal

approximation (Bi, Börner & Chu 1992; Bi & Davidsen 1997; Gnedin & Hui 1996) and the (truncated) Zel'dovich approximation (Doroshkevich, & Shandarin 1977; McGill 1990; Hui, Gnedin, & Zhang 1997). While both approximations are very efficient, they might not be sufficiently accurate. For example, while the one-point density distribution function is close to lognormal for mildly nonlinear fluctuations, the lognormal approximation itself fails to reproduce the density field accurately (Coles, Melott, & Shandarin 1993). The truncated Zel'dovich approximation is somewhat more accurate, and can be used for about a decade in the IGM density, from about $\bar{\rho}/3$ to $3\bar{\rho}$, where $\bar{\rho}$ is the average density of the universe. However, a main drawback of the truncated Zel'dovich approximation is the necessity of the smoothing of the initial density field to minimize the amount of orbit-crossing by the time of interest. This inevitably introduces artificial smoothing of small scale structure, which could bias one's predictions, depending on the quantities one is interested in. While the Zel'dovich approximation can be successfully applied to study the column density distribution of the Lyman-alpha forest (Hui, Gnedin, & Zhang 1997), it remains to be seen whether it can reproduce the detailed results of a hydrodynamic simulation with sufficient accuracy.

In this paper we present a new approximate method, which is based on a standard Particle-Mesh (PM) solver, modified to account for the pressure forces acting on a fluid element. While the PM solver is significantly slower than, say, the Zel'dovich approximation, it is still much faster than a full hydrodynamic simulation. In order to develop a method that will be accurate to within 15% (the reason for this number will be clear by §4), we first in §2 describe two hydrodynamic simulations that we have run to be used as templates against which approximate methods are compared. Then, we start with linear theory to develop some intuition first. In §3 we discuss the effect of the gas pressure on the evolution of linear perturbations. The conventional wisdom that linear baryon (or gas) perturbations are smoothed on the Jeans scale is shown to be incorrect in general, and it is demonstrated that the smoothing scale depends on the reionization history of the universe. Armed with an understanding of the behavior of linear fluctuations, in §4 we compare full hydrodynamic simulations with an approximate method based on combining a PM solver with the appropriate smoothing of initial conditions (with the smoothing scale motivated by the linear analysis), as a way of taking into account the physical effect of gas pressure (this is different from initial smoothing in the case of the truncated Zel'dovich approximation as a way of correcting for orbit-crossing). We then conclude that this method is not sufficiently accurate and proceed to develop our new approximation, which we call Hydro-PM (hereafter HPM) in §5.

The idea of HPM is very simple: one modifies a regular PM solver to compute, in addition to the usual gravitational potential, an effective potential due to the presence of gas pressure. This is possible because there exists a tight correlation between temperature and density (or equivalently, between pressure and density) in the low density limit, which can be computed

Table 1. Cosmological Models

| Model	Ω_0	Ω_b	h	Ω_Λ	σ_8	cell size
LCDM	0.35	0.055	0.7	0.65	0.79	$6.6h^{-1}\,\mathrm{kpc}$
SCDM	1.0	0.05	0.5	0	0.70	$15.6h^{-1}\,\mathrm{kpc}$

quite accurately for any given reionization history (Hui & Gnedin 1997). A given density field then predicts an effective pressure field as well as a definite gravitational potential field. The fundamental rationale is that for the Lyman-alpha forest of sufficiently low column density ($N_{\mathrm{HI}} \lesssim 10^{14}\,\mathrm{cm}^{-2}$), shock-heating is not important (or, equivalently, the density fluctuations are only mildly nonlinear, $\delta \lesssim 10$), which is the one piece of physics that HPM does not incorporate. As we will show, this does not compromise our accuracy significantly while buying us a great increase in efficiency over full hydrodynamic simulations.

It is appropriate that we mention here two wonderful pieces of related work. Petitjean, Mücket & Kates (1995) and Mücket et al. (1996) investigated properties of the Lyman-alpha forest using PM simulations, suitably modified to follow the thermodynamics of baryons. Their approach differ from our HPM method in at least two aspects: the baryons are approximated as following trajectories of dark matter prior to shell-crossing (we include the dynamical effects of pressure on baryons), and shock-heating is modelled in their method which enables them to study higher column density systems. The reader is referred to the above papers for details.

Finally, we conclude in §6 with a brief discussion. A word on our notation: the symbol ρ is used to denote mass density as usual, as well as the mass density in units of the cosmic mean (i.e. ρ and $1 + \delta$ used interchangeably). Which meaning is intended should be clear from the context.

HYDRODYNAMIC SIMULATIONS

We have performed two cosmological hydrodynamic simulations against which we will measure the performance of our approximate methods. We used the SLH-P^{3}M code as described by Gnedin (1995), Gnedin (1996), Gnedin & Bertschinger (1996) and Gnedin & Ostriker (1997). Table 1 contains cosmological parameters of the two models. We have chosen two different models which enable us to test our approximate methods under different conditions. For both models we have used 64^3 baryonic mesh and the softening parameter was set to $1/3$, which gives us a dynamical range of 192. Since we are mainly concerned with modelling the low density IGM, $\delta \lesssim 10$, we do not need to set the softening parameter to a very small value. Our choice of the softening parameter, however, does enable full resolution of regions with $\delta = 10$ or lower. The LCDM model is identical to the model used in our Equation of
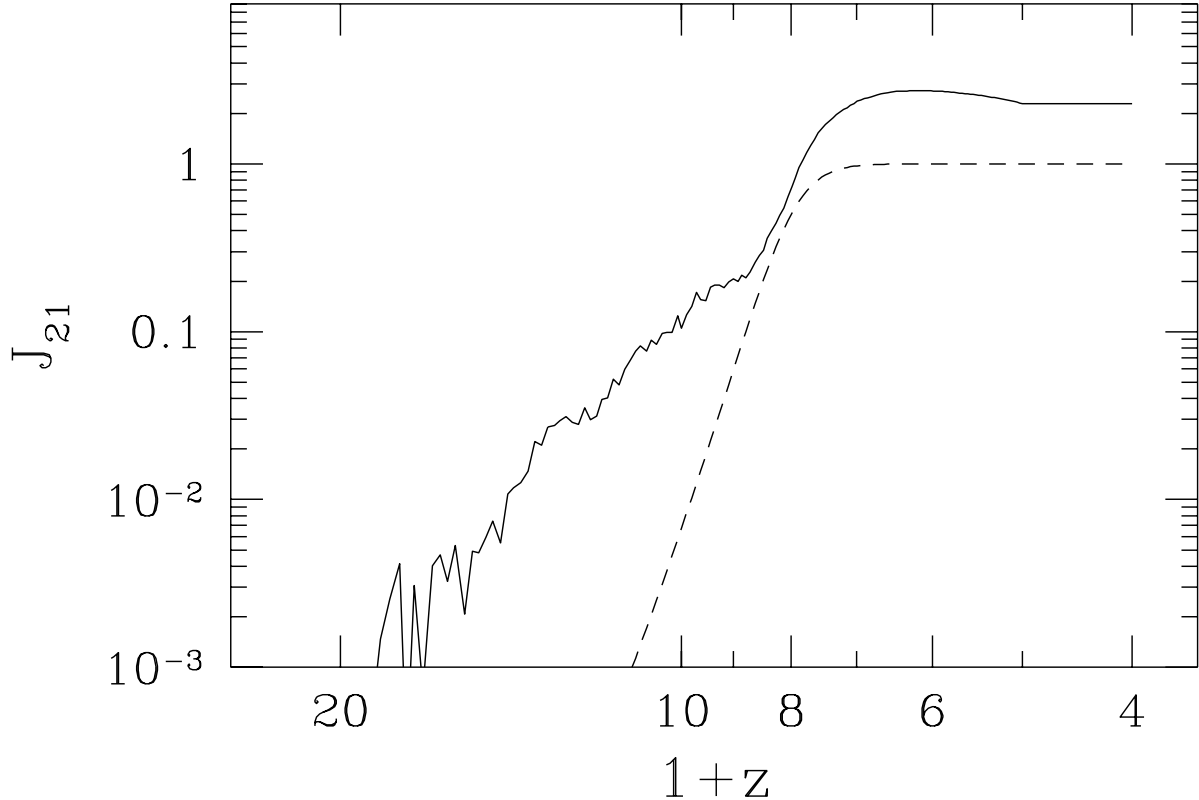
Figure 1. Evolution of the ionizing intensity J_{21} for the LCDM model (*solid line*) and the SCDM model (*dashed line*) as a function of redshift.

State paper (Hui & Gnedin 1997), except for the larger value of the softening parameter, while the SCDM model is close to the model studied by Zhang et al. (1997).

The thermal history for each of our simulations is determined by the evolution of the photo-ionizing background. Figure 1 shows the evolution of the ionizing intensity J_{21} as a function of redshift for both hydrodynamic simulations. The redshift evolution of J_{21} and the spectrum of radiation for the LCDM model was adopted from the simulation described in (Hui & Gnedin 1997). For the SCDM model, we have adopted the following form of the redshift evolution of J_{21}:

$$J_{21}(z) = \frac{1}{2}\left[1 + \tanh\left(100\frac{7-z}{8(1+z)}\right)\right],$$

where J_{21} is defined in exactly the same way as J_{HI} in Hui & Gnedin (1997), and we adopt the same spectral shape as in Hui & Gnedin (1997), equation (7). This form of the redshift evolution of J_{21} is close to the sudden reionization models discussed in detail in Hui & Gnedin (1997). For low z, $z \ll 7$, the ionizing intensity reaches its asymptotic value, $J_{21} = 1.0$, and it drops quickly before the redshift of reionization, $z_{\mathrm{rei}} = 7$. The factor of 100 inside the tanh insures that reionization occurs smoothly in a redshift interval $\Delta z/z \sim 0.01$. This transition

period is introduced to avoid numerical instabilities possible when J_{21} increases abruptly at the redshift of reionization, as in models of sudden reionization.

Both simulations have been continued until $z = 3$. It is worth pointing out that the simulation box in both cases was rather small, $1 h^{-1}$ Mpc for the LCDM model, and $422 h^{-1}$ kpc for the SCDM model. At the final redshift, fluctuations at the box size are already nonlinear, and simulation boxes are not representative patches of the universe. This fact should have minimal effect on the present work: our main goal is to develop an understanding of the relationship between the dark matter and the baryons on small scales, to help us find an approximation that takes into account both gravity and gas pressure in an appropriate manner (on large scales, things are simple: dark matter and baryons simply trace each other). The key is then to resolve structure on the relevant small (mass) scales (as will be explained in the next section), rather than having a representative sample of the universe on large scales.

LINEAR EVOLUTION OF COSMOLOGICAL PERTURBATIONS

The linear evolution of perturbations in the dark matter - baryon fluid is governed by two second order differential equations:

$$\frac{d^2 \delta_X}{dt^2} + 2H \frac{d\delta_X}{dt} = 4\pi G \bar{\rho}(f_X \delta_X + f_b \delta_b),$$

$$\frac{d^2 \delta_b}{dt^2} + 2H \frac{d\delta_b}{dt} = 4\pi G \bar{\rho}(f_X \delta_X + f_b \delta_b) - \frac{c_S^2}{a^2} k^2 \delta_b, \tag{3.1}$$

where $\delta_X(t, k)$ and $\delta_b(t, k)$ are Fourier components of density fluctuations in the dark matter and baryons (we equate baryons with the cosmic gas in this paper) respectively, which have respective mass fractions f_X and f_B, $H(t)$ is the Hubble constant, $a(t)$ is the cosmological scale factor, $\bar{\rho}(t)$ is the average mass density of the universe, $c_S(t)$ is the sound speed in the cosmic gas (where the sound speed is simply defined by $c_S^2 \equiv dP/d\rho$, assuming an equation of state that relates the P and ρ), k is the comoving wavenumber and t is the proper time.

In the limit where the dark matter is gravitationally dominant, $f_b = 0$ in equation (3.1), the growth of δ_X is described by the familiar factor $D_+(t)$ (Peebles 1980), which coincides with $a(t)$ if the matter density of the universe is critical.

The right hand side of the equation for δ_b contains two terms: the gravitational force and the pressure force. On large scales, in the limit $k \to 0$, the pressure force can be neglected, and the baryon fluctuation obeys the same equation as the dark matter fluctuation. Assuming that $\delta_b = \delta_X$ initially, we have

$$\delta_b(t, k \to 0) = \delta_X(t, k \to 0) \propto D_+(t).$$

On small scales, $k \to \infty$, the pressure force is dominant, and one would expect that the baryon fluctuation is suppressed compared to the dark matter fluctuation. A characteristic

scale, where the two forces are equal, is called the Jeans scale. We denote the wavenumber corresponding to the Jeans scale as k_J,

$$k_J = \frac{a}{c_S}\sqrt{4\pi G\bar{\rho}}. \tag{3.2}$$

The Jeans scale is in general a function of time, but for the special case when the gas temperature T evolves with time as $T \propto 1/a$, the Jeans scale is constant in time. In this case, and assuming $f_b = 0$ (i.e. the baryons are gravitationally subdominant), so that $\delta_X \propto D+$, equation (3.1) can be solved analytically:

$$\delta_b(t, k) = \frac{\delta_X(t, k)}{1 + k^2/k_J^2}. \tag{3.3}$$

Thus, at small scales, $k \rightarrow \infty$, the baryon fluctuation is suppressed relative to the dark matter fluctuation by a factor of k_J^2/k^2. Note that this assumes effectively a very special boundary condition: $T \propto 1/a$ *at all times*.

Let us now consider a more realistic case. At sufficiently high redshifts, before the Compton heating of the baryon gas by the CMB becomes inefficient, the evolution of the baryon temperature is well described by the $T \propto 1/a$ law. At redshifts of about 100 (depending on the baryon density of the universe), Compton scattering becomes inefficient and the temperature of the baryon gas drops adiabatically, $T \propto 1/a^2$. By low redshifts, but before the universe reionizes, the gas temperature can be treated as effectively zero (or in other words, the Jeans mass associated with the CMB temperature is too small to be relevant for the modelling of the Lyman-alpha forest).

The gas temperature rises dramatically after the universe reionizes, and its subsequent evolution is obviously our object of interest. As we will show, equations (3.2) and (3.3) no longer provide a correct description of the smoothing and time evolution of the gas.

In order to consider a realistic case, we extract the evolution of the sound speed from our SCDM simulation and solve equation (3.1) numerically with the obtained form of $c_s(t)$.

Figure 2 shows the linear baryon fluctuation, normalized by the linear dark matter fluctuation, at $z = 3$. Three different cases are shown: $f_b = 0.05$ as in the simulation (the solid line), $f_b = 0$ in equation (3.1), baryons being treated as gravitationally subdominant and therefore their gravitational effect is negligible (the dashed line), and $f_b = 1$, all matter being baryonic (the dotted line). The two cases with $f_b = 0.05$ and $f_b = 0$ can barely be distinguished from each other in the figure. The case where all the matter is treated as baryonic also gives a very similar result. This point will be examined further in §6.

Let us focus on the open circles for the time being. They represent the linear baryon fluctuation as given by equation (3.3), where the filtering scale is the Jeans scale as defined in equation (3.2) for $z = 3$. One can see that in this realistic case (where T does not evolve as $1/a$ at all times), filtering of the baryon fluctuation occurs at a smaller scale than the Jeans scale, contrary to conventional wisdom. In addition, oscillations occur at small scales,
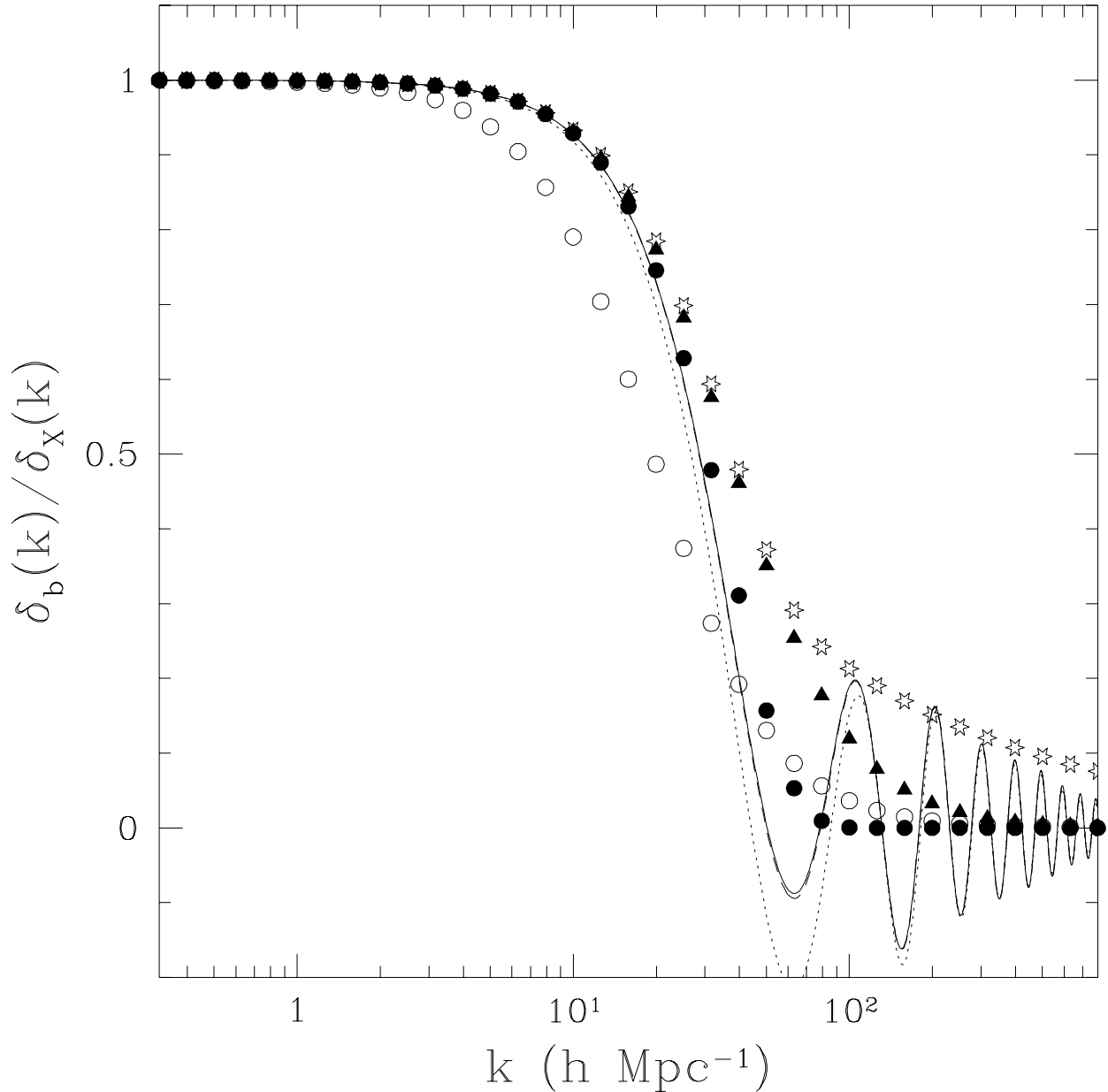
Figure 2. Comparisons of different filtering. The exact linear baryon fluctuation for the SCDM model at $z = 3$ as calculated from equation (3.1) are shown for $f_b = 0.05$ (*solid line*), $f_b = 0$ (*dashed line*, almost overlapping with the *solid line*), and $f_b = 1$ (*dotted line*). Points with different symbols represent different filtering of the linear dark matter fluctuation (to approximate the linear baryon fluctuation): $1/(1 + k^2/k_J^2)$ filtering (*open circles*), $\exp(-k^2/k_F^2)$ filtering (*filled circles*), $1/(1 + k^2/k_F^2)$ filtering (*filled triangles*), and a hybrid filtering which gives the best fit to the envelope of the baryon fluctuation (eq. [4.20]; *stars*).

and the amplitude of these oscillations decay at a rate slower that $1/k^2$, contrary to equation (3.3).

It is possible to understand this analytically. Let us consider the case where the baryons are gravitationally subdominant, $f_b = 0$. Then the dark matter fluctuation simply grows

10

like $D_+(t)$ (ignoring the decaying mode). Let us consider expanding the ratio of the baryon fluctuation to dark matter fluctuation $\delta_b(t,k)/\delta_X(t,k)$ in powers of k^2. Retaining only the first two dominant terms in the small k limit, and recalling that $\delta_b(t,k=0) = \delta_X(t,k=0)$, we have:

$$\frac{\delta_b(t,k)}{\delta_X(t,k)} = 1 - \frac{A(t)}{D_+(t)}k^2,\tag{3.4}$$

where $A(t)$ is an unknown coefficient to be determined. Inserting equation (3.4) into (3.1) and ignoring terms of order k^4 or higher, we obtain the following equation for $A(t)$:

$$\frac{d^2 A}{dt^2} + 2H\frac{dA}{dt} = \frac{c_S^2}{a^2}D_+(t).\tag{3.5}$$

This equation can be easily solved by:

$$A(t) = \int_0^t dt' c_S^2(t')D_+(t')\int_{t'}^t \frac{dt''}{a^2(t'')}.\tag{3.6}$$

where the initial conditions $A(t=0) = dA/dt(t=0) = 0$ are assumed (i.e. no difference between the baryon and dark matter fluctuations at early times). Note that A is positive, which means the baryon fluctuation is *always* suppressed, compared to the dark matter, in the low k regime. We now introduce the *filtering scale*, with the corresponding wavenumber denoted as k_F, by the following expression:

$$A(t) \equiv \frac{D_+(t)}{k_F^2(t)},$$

so that equation (3.4) can now be rewritten as

$$\frac{\delta_b(t,k)}{\delta_X(t,k)} = 1 - \frac{k^2}{k_F^2}.\tag{3.7}$$

The following expression for the filtering scale k_F can be obtained:

$$\begin{aligned}
\frac{1}{k_F^2(t)} &= \frac{1}{D_+(t)}\int_0^t dt' a^2(t')\frac{\ddot{D}_+(t') + 2H(t')\dot{D}_+(t')}{k_J^2(t')}\\
&\quad \int_{t'}^t \frac{dt''}{a^2(t'')},
\end{aligned}\tag{3.8}$$

where we have replaced the sound speed by its expression in terms of the Jeans scale at the same moment (eq. [3.2]), and dot denotes differentiation with respect to the time t.

An important conclusion follows from equation (3.8). Let us rewrite it in the following form, using the median value theorem:

$$\begin{aligned}
\frac{1}{k_F^2(t)} &= \frac{1}{k_J^2(t_*)}\left[\frac{1}{D_+(t)}\int_0^t dt' a^2(t')\right.\\
&\quad \left.\left(\ddot{D}_+(t') + 2H(t')\dot{D}_+(t')\right)\int_{t'}^t \frac{dt''}{a^2(t'')}\right],
\end{aligned}$$

where t_* is between 0 and t. The expression in square brackets integrates to 1, and we obtain:

$$k_F(t) = k_J(t_*),$$
<div align="right">(3.9)</div>

where $t_* \leq t$. In other words, the filtering scale at a given time is equal to the Jeans scale at some earlier time. In particular, if the Jeans scale $1/k_J$ is an increasing function of time, which is typically the case for sufficiently low redshifts after reionization, the filtering scale $1/k_F$ is always *smaller* than the Jeans scale. The reverse would be true prior to reionization, as we will see in a moment.

The above notion of the filtering scale is, strictly speaking, only applicable in the small k limit, because it is derived based on an expansion in k^2 (equation [3.4]). To see how well this filtering scale provides a description of the linear baryon fluctuation in the high k regime, we show in Fig. 2 with filled circles the filtering in the form $\exp(-k^2/k_F^2)$ (i.e. $\delta_b = \delta_X \exp[-k^2/k_F^2]$), where k_F is computed from equation (3.8) using the evolution of the sound speed (or in other words the Jeans scale) as extracted from the SCDM hydrodynamic simulation.

One can see despite the fact that k_F is derived in the small k limit, the exponential filtering with k_F gives an excellent fit to the baryon fluctuation even for high k, until oscillations take over. We also show with filled triangles the filtering of the form $1/(1 + k^2/k_F^2)$ (i.e. $\delta_b = \delta_X/[1 + k^2/k_F^2]$) for the same k_F, which gives a worse fit for the high k cut-off and, as in the case of $\exp(-k^2/k_F^2)$ filtering, does not match the envelope of oscillations on small scales.

Encouraged by the excellent performance of the gaussian filtering on scale of $1/k_F$ in reproducing the exact linear solution, we now consider a few special cases, where k_F can be calculated analytically. Let us restrict ourselves to an $\Omega_0 = 1$ universe, where $D_+(t) = a(t)$. For simplicity, we will assume that the mean molecular weight of the cosmic gas does not change, in which case the sound speed is directly proportional to the square root of the gas temperature. First, we consider the case where the gas temperature T is zero before reionization (which occurs at $a = a_{\rm rei}$), and remains constant thereafter:

$$T = \begin{cases} 0, & a < a_{\rm rei}, \text{ and} \\ T_0, & \text{otherwise.} \end{cases}$$
<div align="right">(3.10)</div>

Computing the integral (3.8), we obtain for $a > a_{\rm rei}$:

$$\frac{1}{k_F^2} = \frac{1}{k_J^2}\frac{3}{10}\left[1 + 4\left(\frac{a_{\rm rei}}{a}\right)^{5/2} - 5\left(\frac{a_{\rm rei}}{a}\right)^2\right].$$
<div align="right">(3.11)</div>

In particular, for $a \gg a_{\rm rei}$,

$$k_F = \sqrt{\frac{10}{3}}k_J.$$

Another instructive example is when the gas temperature decays as $1/a$ after reionization,

$$T = \begin{cases} 0, & a < a_{\rm rei}, \text{ and} \\ T_0 a_{\rm rei}/a, & \text{otherwise.} \end{cases}$$
<div align="right">(3.12)</div>

12

In this case the filtering scale for $a > a_{\text{rei}}$ is given by

$$\frac{1}{k_F^2} = \frac{1}{k_J^2} \left[1 + 2 \left(\frac{a_{\text{rei}}}{a} \right)^{3/2} - 3 \frac{a_{\text{rei}}}{a} \right]. \qquad (3.13)$$

In the limit $a \gg a_{\text{rei}}$ we recover the standard result $k_F = k_J$, but the asymptote is reached only slowly, and even at $z = 3$ and for $z_{\text{rei}} = 7$, we obtain $k_F = 2.2 k_J$. We emphasize the departure of the correct filtering scale from the usual Jeans scale is a result of the fact that T above is not assumed to evolve as $1/a$ at all times. The time evolution of T considered above is partly motivated by reionization models in which the originally cool cosmic gas was heated up to a high temperature by radiation emitted by sources (stars, quasars, etc) that turned on at some high redshift.

Typically, the gas temperature decays as an intermediate power between a^0 and a^{-1} after reionization (Hui & Gnedin 1997). We, therefore, conclude that in a realistic case one should expect that at $z \sim 3$ the filtering scale of the cosmic gas is about a factor of $1.5 - 2.5$ smaller than the Jeans scale, unless the universe reionized at a very high redshift, $z_{\text{rei}} \gg 10$.

Another interesting example is the evolution of the baryon perturbations before reionization. After recombination at $z \sim 1200$, the cosmic gas temperature is still coupled to the CBR temperature by Compton heating, and therefore evolves as $T \propto 1/a$. At a later time $a_{\text{dec}} = 0.01(\Omega_b h^2/0.0125)^{2/5}$, Compton heating becomes inefficient, and the gas temperature decreases adiabatically, $T \propto 1/a^2$. Since the Jeans scale decreases with time for an adiabatically cooling gas, the filtering scale for the cosmic gas is actually *larger* than the Jeans scale. More precisely, a good approximation to the evolution of the cosmic gas temperature is given by the following expression:

$$T = \begin{cases} 2.73 \, \text{K}/a, & a < a_{\text{dec}}, \text{ and} \\ 2.73 \, \text{K} a_{\text{dec}}/a^2 & \text{otherwise.} \end{cases} \qquad (3.14)$$

In this case the filtering scale for $a > a_{\text{dec}}$ is given by

$$\frac{1}{k_F^2} = \frac{1}{k_J^2} \left[3 \ln(a/a_{\text{dec}}) - 3 + 4 \left(\frac{a_{\text{dec}}}{a} \right)^{1/2} \right]. \qquad (3.15)$$

For example, for $\Omega_b h^2 = 0.0125$, $k_F = 0.45 k_J$ at $z = 10$, and in term of masses, the characteristic mass scale on which the gas distribution is smoothed, $M_F \propto 1/k_F^3$, is about 11 times *larger* than the Jeans scale, $M_J \propto 1/k_J^3$. This result has important implications for understanding the formation of the first bound objects in the universe.

Next, we turn our attention to the oscillations in the high k regime, a behavior we can understand analytically for the time evolution specified in equation (3.12). We can solve equation (3.1) exactly in this case, assuming once again the case of an $\Omega_0 = 1$ universe with $f_b = 0$ (i.e. baryons being gravitationally subdominant):

$$\frac{\delta_b(t, k)}{\delta_X(t, k)} = \frac{1}{1 + k^2/k_J^2} \left(1 + \frac{k^2}{k_J^2} \left[\frac{n_-}{n_- - n_+} \left(\frac{a}{a_{\text{rei}}} \right)^{n_+} - \right. \right.$$

$$\frac{n_+}{n_- - n_+} \left(\frac{a}{a_{\rm rei}}\right)^{n_-}\right]\right) \tag{3.16}$$

for $a > a_{\rm rei}$, where

$$n_\pm = -\frac{5}{4} \pm \frac{3}{4}\sqrt{\frac{1}{9} - \frac{8}{3}\frac{k^2}{k_J^2}},$$

and where δ_X grows as a. Note that since $T \propto 1/a$ at $a > a_{\rm rei}$, the Jeans scale k_J is constant in time. In the limit $a \gg a_{\rm rei}$ and for k sufficiently small, equation (3.16) reduces to equation (3.3).

Let us now consider a fixed final a, and take the large k limit. Then both n_+ and n_- become complex (but δ_b is still real), and δ_b as a function of k oscillates. However, one can see that in the high k limit, the amplitude of these oscillations is independent of k. We, therefore, conclude that in general δ_b/δ_X has no power-law asymptote in the high k limit. It is sometimes claimed in the literature that δ_b/δ_X always approaches an asymptote of k^{-2} in the high k limit. That statement is only correct if T evolves as a fixed power law in a at *all times* (see Bi et al. 1992 for derivation). The simple case above provides an example of departure from this property.

Finally, we emphasize that the two hydrodynamic simulations described in the previous section have sufficiently small cell sizes so that the corresponding correct filtering scales $(1/k_F)$ are resolved by about 5 mesh cells. This ensures that we can meaningfully compare different smoothing prescriptions, as explained in the following section.

FILTERING INITIAL CONDITIONS FOR A PM SIMULATION

The linear analysis in the previous section shows that the two mass components, the dark matter and the cosmic gas, evolve differently on small scales: the dark matter is affected by gas pressure only via gravitational interaction with the gas, while the gas evolution is directly influenced by the thermal pressure on sufficiently small scales. In order to compute this complex interaction in every detail, a two-component hydrodynamic simulation is needed. But often the precision achieved by the full hydrodynamic simulation is not required. For instance, current observations of the Lyman-alpha forest typically give about 10-15% accuracy for the column density distribution. We will attempt to develop an approximation, that is significantly faster than a hydrodynamic simulation, but at the same time gives us results with similar accuracy.

As a step toward this goal, we will concentrate in this paper on single-component approximations, i.e. approximations where the evolution of the cosmic gas is computed using only one set of resolution elements (in our case particles) instead of following both the dark matter and the gas separately. This approach is certainly more economical than a full hydrodynamic simulation, but the question is: can we make it accurate enough?

14

It is certainly possible to emulate a gas-dynamic solver using a simple dark matter solver in the linear regime. Let $\delta_X^{(0)}(t, k)$ and $\delta_b^{(0)}(t, k)$ be the linear solutions to equation (3.1) for a specific cosmological model. Suppose we are interested in the baryon fluctuation at some final moment $t = t_f$ (which is early enough so that the fluctuation remains linear). Let us model the evolution of the baryon perturbation with a dark-matter-only solver (e.g. PM), which, in the linear regime, is equivalent to solving the first of equations (3.1) and assuming $f_b = 0$. If we choose the following initial condition for the dark-matter-only solver at an early time $t = t_i$:

$$\delta_X(t = t_i, k) = \frac{D_+(t_i)}{D_+(t_f)} \delta_b^{(0)}(t = t_f, k),\tag{4.17}$$

it is easy to see that we will reproduce the baryon fluctuation in the linear regime at $t = t_f$. Since, as we have shown in the last section, $\delta_b^{(0)}(t = t_f, k)$ can be modelled by $\delta_X(t = t_f, k)$ multiplied by some suitable filter, the above initial condition is equivalent to smoothing the initial δ_X with the same filter.

One might then hope to model the dynamical evolution of the gas by a PM simulation, with the initial conditions appropriately smoothed. In other words, one may try to model the gas evolution under the assumption that the gas is influenced by gravity alone, hoping that the initial filtering procedure is sufficient to model the effect of pressure.

There is no guarantee that this simple-minded method would work. After all, our idea of a simple filtering scale is derived from linear analysis, while for our applications, we are interested in regions of space with overdensity below, but reaching up to about 10. In fact, we will show in this section that this method works to a certain extent, but is *not* good enough, i.e. it fails to achieve an accuracy of $10 - 15\%$ in a point-by-point comparison of density and velocity fields against full hydrodynamic simulations. Observationally, interesting quantities such as the column density distribution are typically measured with an accuracy of about $10 - 15\%$. As we will show in the next section, this level of accuracy requires similar accuracies in the density and velocity fields themselves.

Before we embark upon a quantitative comparison of the PM + filtering method versus hydrodynamic simulation, we have to address one technical point.

A collisionless (alias "N-body") numerical simulation, such as PM, uses particles to follow the evolution of the system. For our applications, it is eventually necessary to compute the gas density and velocity as a function of spatial positions. How does one convert a distribution of particles into, say, the density field? There exist several techniques, but in this paper we will adopt the simplest method of assigning the density onto a uniform mesh using particle weights. Specifically, we will use the Triangular-Shape-Clouds (TSC) scheme to assign the particle density onto a mesh. This method, however, suffers from numerical noise. For example, in a sufficiently underdense region a particle might be so remote from its neighbors that the TSC assignment would leave empty regions (zero density) between

the particle and some of its neighbors. This generates unphysical structure on small scales. The easiest way to suppress this numerically generated structure is to smooth the resultant density distribution with, for example, a gaussian filter. However, since we are trying to achieve an order of 10-15% accuracy in reproducing the gas distribution, we ought to ensure that we reduce the numerical assignment noise to within a couple of percent. In other words, what is the degree of smoothing we must apply to the TSC-assigned density distribution to reduce the noise to, say, 2%?

In order to answer this question, we have performed two PM simulations: a low resolution one with 64^3 mesh, and a high resolution one with 128^3 mesh with the same number of particles (64^3) and identical initial conditions. The rms overdensity at the final moment is chosen to be 3 to allow for development of sufficient nonlinearities. Those two simulations therefore should produce the same final density distribution except that the high resolution simulation has twice higher spatial resolution. The two density distributions are then smoothed with a gaussian filter with some chosen smoothing scale. By comparing the two simulations smoothed with varying smoothing scale, we find that the smoothing scale should be at least 3 cells to reduce the numerical assignment noise to within 2%. This conclusion has also been confirmed by Bertschinger (1997).

Therefore, from now on, we will present results of collisionless N-body experiments with the final density and velocity fields assigned to the uniform mesh by the TSC scheme and then smoothed with a gaussian filter of three mesh cells. This procedure is admittedly quite wasteful, since it implies that we lose a factor of 1.5 to 3 in spatial resolution. The advantage is that it is simple to implement. We defer developing a more efficient density assignment scheme to future work.

Before we move on to testing various forms of PM + initial filtering, it is interesting to address the question of whether we need any initial smoothing at all, i.e. how much the dark matter and the gas densities differ in a hydrodynamic simulation. Figure 3 shows the scatter plot of the dark matter versus gas density for the SCDM hydrodynamic simulation at $z = 3$. One can see that the difference is significant, with the dark matter density being a factor of 3 lower than the gas density in the lowest density regions. Hence, a pure PM simulation, with no modifications to mimic the dynamical effects of pressure, would fail to reproduce the gas distribution of the low density IGM with sufficient accuracy.

We now turn to testing the method of combining PM with the filtering of the initial conditions, as stated at the beginning of this section. A hydrodynamic simulation is run for the SCDM model as described in Table 1. All PM simulations are performed with 64^3 particles on a 192^3 mesh for the same model. The choice of the mesh size of 192^3 is a natural one given that the hydrodynamic simulation has 64^3 moving mesh and the softening parameter is set to 1/3 (we have in fact tested different mesh sizes, from 64^3 to 256^3, and found that the 192^3 mesh gives, as could be expected, much better agreement with the
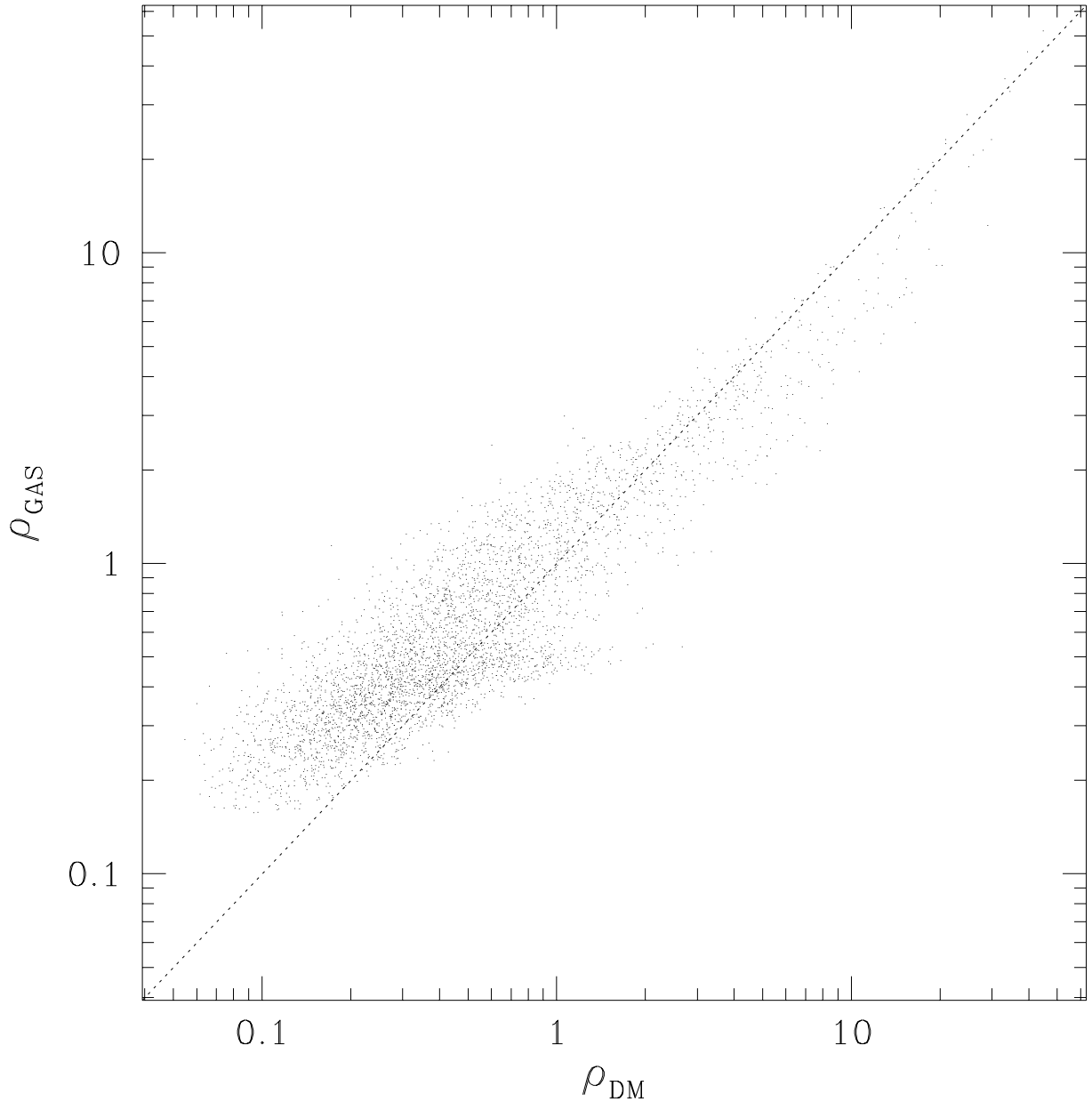
Figure 3. A scatter plot of the dark matter density vs the gas density (in units of respective average densities) in the SCDM hydrodynamic simulation at $z = 3$. Because of finite gas pressure, the gas distribution does not reach densities as low as those of the dark matter.

hydrodynamic simulation). The pre-filtered initial conditions of the PM simulations are chosen to be exactly the same as those in the hydrodynamic simulation.

Figure 4 summarizes our findings. Before we proceed further, a few words are in order on our way of presenting comparisons between two three-dimensional fields (say, density or velocity fields). The easiest way for such a comparison is a scatter plot, similar to one presented in Fig. 3. However, while a scatter plot is sufficiently illustrative, it fails to give

explicit quantitative information. We, therefore, use the following method of comparing two fields hereafter in this paper. For definiteness, suppose we are interested in the field $Q(\boldsymbol{x})$ (which could be density, velocity or the spectrum; in the case of spectrum, $\boldsymbol{x}$ would be replace by λ the wavelength). We denote by Q_{EXACT} the field taken from one of the two hydrodynamic simulations, and by Q_{APPROX} the field taken from the approximate computation under consideration. Then we identify all spatial points in the relevant hydrodynamic simulation which have the value of Q_{EXACT} within ± 0.05dex from some chosen value Q_0, and compute the following average:

$$[Q_{\mathrm{APPROX}} - Q_{\mathrm{EXACT}}]_{\mathrm{AVG}} \equiv$$
$$\langle Q_{\mathrm{APPROX}}(\boldsymbol{x}) - Q_{\mathrm{EXACT}}(\boldsymbol{x}) \rangle |_{Q_{\mathrm{EXACT}}(\boldsymbol{x})=Q_0} \tag{4.18}$$

and the rms deviation:

$$[Q_{\mathrm{APPROX}} - Q_{\mathrm{EXACT}}]_{\mathrm{RMS}} \equiv$$
$$\sqrt{\langle (Q_{\mathrm{APPROX}}(\boldsymbol{x}) - Q_{\mathrm{EXACT}}(\boldsymbol{x}))^2 \rangle |_{Q_{\mathrm{EXACT}}(\boldsymbol{x})=Q_0}} \tag{4.19}$$

over the ensemble of Q_{APPROX}'s at the corresponding spatial points in the approximate calculation. The above quantities would then be plotted as a function of Q_0. In the case of density, we use $Q = \ln\rho$ where ρ is measured in units of the cosmic average; for the spectrum, we use $Q = F/(1 - F_{\mathrm{EXACT}})$ where F is the transmission; for velocity v, we use $Q = v/v_m$ where v_m is defined in Figure 6. In all cases, the average and rms deviations defined above provide quantitative measures of the *fractional* error in the corresponding approximate method, compared against the hydrodynamic simulation.

Given the two deviations, the average one, and the rms one, which one is more important? The average deviation can be interpreted as a systematic error: it measures how much the "approximate" density field systematically deviates from the "exact" density field. Obviously, it is desirable to reduce this error as much as possible. The rms deviation is more like a random error, and while it is also desired to be as small as possible, a larger value of the random error can perhaps be tolerated. In comparing simulations with observations, usually a statistical quantity is computed by averaging the results of simulations in some fashion. This averaging will reduce the random (rms) error, but may not reduce the systematic (average) error. Therefore, as we are proceeding with our tests, we will try to reduce the average error to about 5%, and then try to reduce the rms error as much as possible while keeping the average error small. We again emphasize that we will concentrate on the density range $\rho \lesssim 10$, and will ignore all possible error induced in the high density regions.

Our ultimate object of interest is of course a comparison of the gas distributions between two methods, but let us take a look at the dark matter distributions first. There are a few interesting observations.

The agreement between the dark matter density from the hydrodynamic simulation and

the density from a PM simulation with identical initial conditions (no pre-filtering for this PM simulation; shown with solid lines in Fig. 4) is better than 4 percent on average, and about 5% rms, getting to 10% at overdensities about 10. At higher overdensities the agreement gets worse. What is the reason the two dark matter distributions do not agree, in spite of the fact that the formal resolutions of two simulations are matched? This disagreement is caused by the difference in Green functions used to compute the gravity force in two simulations. While the hydrodynamic simulation has the Green function corresponding to the Plummer softening, the PM simulations have the Green function corresponding to our specific choice of density assignment on the PM mesh. This difference in Green functions, which is purely methodological, induces error of up to 10% rms even for $\delta \sim 10$ (in particular, stronger deviation at higher density is due to the fact that the Plummer Green function is slightly softer than our PM Green function).

Finally, we turn our attention to a comparison of gas density distributions. We first consider the simplest variant of the PM + filtering method: we smooth the initial conditions with the $\exp(-k^2/k_F^2)$ filter (i.e. $\delta(k) \rightarrow \delta(k)\exp[-k^2/k_F^2]$), where k_F is given by equation (3.8) with k_J related to the sound speed through (3.2), and the evolution of the sound speed simply taken from the hydrodynamic simulation. Recall that this particular choice of filtering gives an excellent fit to the exact linear baryon fluctuation on large scales (filled circles in in Fig. 2). One might hope that the same form of filtering + PM gives an adequate approximation even in the mildly nonlinear regime.

This case is shown by the dotted lines in Fig. 4. Note that while the average error is small for $0.5 \lesssim \rho \lesssim 10$, it gets significantly worse at $\rho \sim 0.1$, and the rms error is as high as 20% almost everywhere. What causes the strong differences in low density regions? More specifically, in such regions, why does the hydrodynamic simulation predict gas densities substantially lower than the PM + smoothing approximation? One possible explanation is that the choice of initial filtering is incorrect: the $\exp(-k^2/k_F^2)$ filtering underestimates the amount of power at high k. From the linear analysis shown in Fig. 2, it can be seen that this filter fails to take into account extra power due to oscillations in the large k limit.

We therefore try two other variants of the PM + filtering method. One is using the $1/(1 + k^2/k_F^2)$ filter (shown as filled triangles in the linear analysis of Fig. 2). Its results, as compared against the hydrodynamic simulation, are shown with the long-dashed lines in Fig. 4. This choice of filtering gives a slower cut-off at high k compared to the gaussian filter. The average agreement at low densities significantly improves with this form of filtering, at the expense of, however, increased rms error and average error at higher densities.

Finally, the short-dashed lines in Fig. 4 show the results of the PM + filtering method with the following filter function:

$$f_b(t,k) = \frac{1}{2}\left[e^{-k^2/k_F^2} + \frac{1}{\left(1 + 4k^2/k_F^2\right)^{1/4}}\right]. \tag{4.20}$$

This choice of filtering gives a very good fit to the envelope of oscillations at high k in the linear fluctuations (the star symbols in Fig. 2). One can see that the average error still reaches 10% within the range $\rho < 10$, and the rms error is as high as 30% for intermediate densities.

We have tried quite a few other forms of filtering the initial conditions, each giving effectively different amounts of power at high k, but none of them reduces the average nor the rms error substantially.

We believe the fundamental flaw of the above PM + filtering procedure is that a single uniform smoothing scale is assumed for the whole density field. This is adequate in the linear regime where spatial fluctuations of the temperature can be ignored in computing the filtering scale (i.e. these fluctuations contribute to terms of higher order than those in equation [3.1]). But in the mildly nonlinear regime, one can no longer ignore such fluctuations. In fact, places with higher density tends to have higher temperature (Hui & Gnedin 1997), and hence higher pressure and more smoothing. One then expects the lower density regions, because of their lower thermal pressure, to be less smoothed compared to the higher density regions (but confined to $\rho \lesssim 10$). A uniform smoothing procedure would tend to overestimate the density in the lowest density regions. Note that the PM part of our procedure does effectively introduce non-uniform smoothing, but it does not do so in a way that mimics the action of thermal pressure correctly.

We are not aware of a computationally efficient way of performing the necessary variable smoothing on a large mesh. Should such an algorithm be invented, the case for the PM + initial-filtering may be reconsidered, but at the moment we must admit that this simple method fails to give us the desired accuracy in reproducing results of the full cosmological hydrodynamic simulation, and we must search for something better.

HYDRO-PM APPROXIMATION FOR THE COSMIC GAS DISTRIBUTION

We have repeatedly emphasized in this paper that dynamically, the main difference between dark matter and gas is that the latter is subject to thermal pressure on top of gravity. A hydrodynamic code is designed to compute this thermal pressure and in general, there is no other alternative. However, in case of the low density IGM, a very useful fact can be exploited to our advantage: there exists a tight correlation (to better than 10%) between gas density and temperature (and hence pressure as well) in the low density regime (Hui & Gnedin 1997), where shock-heating is not important. The density-temperature relation is well-described by a power-law equation of state:

$$T = T_0 \rho^{\gamma-1}, \tag{5.21}$$

where T_0 is a constant of the order of 10^4K, and γ is typically about $1.4 - 1.6$. Both T_0 and γ evolve with time in a way that depends on reionization history, but we have developed an efficient method to predict them with high accuracy (Hui & Gnedin 1997).

The equation of state given above immediately provides us with the thermal pressure once the gas density is known. The need in the hydrodynamic solver suddenly evaporates, and the gas evolution can now be followed with a PM-type solver, provided it is modified appropriately to include the effect of thermal pressure. We show below how this can be done.

Let us consider the equation of motion for a cosmic gas element:

$$\frac{d\boldsymbol{v}}{dt} + H\boldsymbol{v} = -\nabla\phi - \frac{1}{\rho}\nabla P, \tag{5.22}$$

where $\boldsymbol{v}$ is the gas peculiar velocity, ϕ is the gravitational potential, and P is the thermal pressure. If the gas is highly ionized (so that the mean molecular weight is roughly constant, which is true for the Lyman-alpha forest), and the temperature is a function of density only, so that $P = P(\rho)$, equation (5.22) can be reduced to the following equation:

$$\frac{d\boldsymbol{v}}{dt} + H\boldsymbol{v} = -\nabla\psi \tag{5.23}$$

where

$$\psi = \phi + \mathcal{H}, \tag{5.24}$$

and $\mathcal{H}$, called *the specific enthalpy*, is

$$\mathcal{H}(\rho) = \frac{P(\rho)}{\rho} + \int_1^\rho \frac{P(\rho')}{\rho'}\frac{d\rho'}{\rho'}.$$

Equation (5.23) is identical to the equation of motion for the collisionless dark matter except that the usual gravitational potential ϕ is replaced by an effective potential ψ, which takes into account both gravity and thermal pressure. Since the gravitational potential ϕ has to be computed from the density field in a regular PM simulation anyway, it adds only a modest computational overhead to compute the enthalpy as well. It is extremely simple to modify the regular PM routine to do so, and we will call this method the "Hydro-PM", or HPM.

In principle, one should then follow the motion of two sets of particles: the gas which follows the equation of motion as in (5.23) and the dark matter which obeys the same equation except that $\mathcal{H} = 0$. In practice, to reduce the computational cost, we treat both sets of particles as if they all follow the same equation of motion (equation [5.23], with the full ψ including both gravity and pressure). This might seem quite unjustified. But one should bear in mind that on large scales, pressure is not dynamically important, and so allowing pressure to also act on the dark matter particles makes practically no difference. The same cannot be said for small scales: the artificially imposed pressure on dark matter causes its distribution to be less clustered than it should be. It then becomes a question of how sensitive the small scale pressure (which is dynamically more important than gravity

on the same scales) on the baryons is to the detailed distribution of matter. The answer seems to be: not very much, but we would come back to this point in the last section. For now, the reader can take this single component HPM method as a plausible approximation, the merits of which can only be weighed through detailed comparisons with hydrodynamic simulations.

There is however an important technical point that we should discuss before going onto tests of the HPM method. In a PM (or HPM) code, the density is assigned onto a mesh using the TSC assignment scheme, as an intermediate step in the computation of the potential ϕ (or ψ). As we pointed out at the beginning of the previous section, this induces numerical noise on small scales (high k). This noise is not significant for the gravity calculation, since it is suppressed by k^{-2} power in the computation of the gravitational potential ($\phi(k) \propto k^{-2}\delta(k)$). The computation of the gas enthalpy, however, does not include such suppression, and the numerical noise could be a problem. We therefore smooth the gas density according to the prescription (over three mesh cells) developed at the beginning of the previous section (in other words, we smooth the density field not only at the final moment, but also at the intermediate steps of the force calculation). As a result, the pressure force is suppressed on scales below about three cell sizes. It is then important that we resolve the scale $1/k_F$ by at least three cells (assuming the linear filtering scale $1/k_F$ gives the approximately correct scale over which the density field is physically smoothed due to pressure). Otherwise, the artificially reduced pressure at scales below three cells (because of our smoothing procedure to reduce numerical noise) could lead to unphysical clustering on those scales.

In the limit when the filtering scale is very small, and is below the cell size, the pressure effect will be insignificant. One then may consider running just a pure PM simulation to avoid the additional computational expense of about 25% because of the HPM modification.

Let us proceed to the comparison of the HPM approximation with full hydrodynamic simulations. We extract the equations of state as a function of redshift from our hydrodynamic simulations and use them in the HPM simulation (the equations of state thus obtained agree very well with those obtained using the method of Hui & Gnedin 1997; we use for HPM the exact equations of state from the hydrodynamic simulation so that we can focus on the error induced by the approximate dynamics in HPM). Figure 5 shows the average and rms errors for the HPM vs full hydrodynamic simulation for the SCDM model at three different epochs and for the LCDM model at $z = 3$. We also show for each panel the corresponding value of σ_F, which is the rms linear overdensity for the $\exp(-k^2/k_F^2)$ filter:

$$\sigma_F^2 = \frac{1}{2\pi^2} \int_0^\infty dk\, k^2 P_L(k, a) \exp(-2k^2/k_F(a)^2), \tag{5.25}$$

where $P_L(k, a)$ is the linear power spectrum of a given model at a given value of the scale factor a, $1/k_F(a)$ is the filtering scale at the same moment given by equation (3.8) (σ_F grows slower that a because k_F increases with time), and the factor of 2 in the exponential comes

from relating δ to the power spectrum by $P_L(k) \propto \delta^2(k)$. The quantity σ_F therefore measures the degree of nonlinearity of the gas distribution in the model. At $z = 3$, the SCDM model is at a more nonlinear state than the LCDM model.

We also show in Fig. 5 two variants of the PM + filtering methods from Fig. 4 for comparison.

Note that HPM gives a significantly better fit to the gas density distribution than the PM + filtering approach. For $\delta \lesssim 10$, the average error generally stays within 5%, and the rms error is only weakly dependent on density and is about 15% for high σ_F cases, and falling to about 10% for low σ_F cases [‡]. This is an important improvement over the PM + filtering method.

The gas density is not the only quantity that we would like to model. For the purpose of generating absorption spectrum, it is important that we have sufficiently accurate velocities as well. Figure 6 shows the comparison between one-dimensional gas velocities (velocities projected along some fixed direction) in the HPM approximation and in the full hydrodynamic simulation for our SCDM model (the solid line). The quantities on the y-axis in Figure 6 are supposed to reflect the average and rms *fractional* errors in the velocity. The division by σ_v for small $|v_{\mathrm{EXACT}}|$ is implemented to avoid arbitrary blow up of the fractional error when the velocity vanishes. The HPM approximation reproduces the gas velocity again to within 15% rms error, but the average (systematic error) has now increased to more than 10% for velocities in excess of two sigma. This is an expected result, since high velocities generally correspond to the high density regions, where the HPM approximation breaks down (because shock-heating destroys the tight correlation between density and temperature/pressure). We also show for comparison results of the PM + filtering approximations, which cannot quite match the performance of HPM.

Since we plan to apply the HPM approximation to model the Lyman-alpha forest, we must also verify that no significant systematic error is introduced in the absorption spectra themselves. We generate spectra along randomly oriented lines-of-sight through the hydrodynamic and the HPM simulations, and show three examples in Figures 7-9. The first line-of-sight passes through an underdense region, the second passes through an overdense region with overdensities $\delta \sim 5$ (the HPM method is expected to give accurate results in this case), and the third passes through a peak with the overdensity $\delta \sim 16$. The HPM method is expected to make a larger error in the third case, and this can be easily observed in the corresponding bottom and middle panels, for density and velocity fields. However, since the transmission F is related to the optical depth τ by $F = e^{-\tau}$, and the optical depth is in

---

[‡] The LCDM model shows slightly worse agreement at $5 \lesssim \delta \lesssim 10$. This is mostly due to the fact that we saved fewer intermediate data while running this simulation, and as the result, the evolution of the equation of state from this simulation is determined less accurately than the respective evolution from the SCDM simulation.

turn approximately proportional to density to some power, a relatively large error in density produces only a relatively small error in F.

To further quantify this, we show in Figure 10 comparisons between the decrements $(1 - F)$ in the full hydrodynamic simulation and the HPM approximation computed from 300 random lines-of-sight. Since the neutral hydrogen fraction, and therefore the decrement at a given wavelength, depends on the ionizing intensity J_{21}, we show two different cases: $J_{21} = 0.3$ (the solid line) and $J_{21} = 0.5$ (the dashed line). Both values are too high for this model to reproduce the observed column density distribution of the Lyman-alpha forest. Lower values of the ionizing intensity will improve the agreement, since in this case a given value of the decrement will correspond to a lower value of the gas density.

One might also wonder if the above comparisons underestimate the actual error, because of the small simulation box size: the thermal broadening could drastically reduce discrepancies, because the broadening width is a fair fraction of the box size in wavelength space. To test this possibility, we recompute the spectrum for the same lines of sight through the HPM and the full hydrodynamic simulations with $J_{21} = 0.5$, but with the gas temperature reduced by a factor of 100. The corresponding comparison is plotted in Fig. 10 with the dotted line. One can see that thermal broadening cannot explain the small errors in the transmitted flux.

Figure 10 clearly shows the range of applicability of the HPM approximation. While the average error stays within 10 %, the rms error is smaller than about 18 % throughout the whole range of decrement. A remarkable feature of the HPM approximation is that it actually describes regions of high decrements rather well. This is because even though the HPM method fails to give the right density field with sufficient accuracy in high density regions, its errors are effectively suppressed because the same regions give rise to saturated absorption lines.

As we have emphasized before, in comparing simulations with observations, usually a statistical quantity is computed by averaging the results of simulations in some fashion, which tends to reduce the random (rms) error (in other words, the point-by-point comparisons above are a rather stringent test). We show one interesting example in Figure 11, namely the column density distribution. We compute the column density distributions of the full hydrodynamic simulation and the HPM approximation for our SCDM model at $z = 3$ using the Density-Peak Ansatz (Gnedin & Hui 1996; Hui, Gnedin, & Zhang 1997). Both column density distributions are plotted in Figure 11 with the solid and dotted lines respectively. We also add a 10% error-bar to the column density distribution of the full hydrodynamic simulation for illustrative purpose. Note that the two distributions agree to within about 13%, and the best-fit slopes differ by less than 3%. We thus conclude that the HPM approximation can be successfully used to model the Lyman-alpha forest when a 10-15% accuracy is sufficient.

DISCUSSION

We have demonstrated that the HPM method, based on a modified PM routine to take into account the dynamical effect of pressure as well as gravity, is an efficient and accurate alternative to hydrodynamic simulations in predicting the density and velocity fields, as well as absorption spectra.

The key that makes the HPM method possible is the fact that in the low density regime, where shock-heating is not important, there exists a tight correlation between density and temperature/pressure. The almost one-to-one relationship between these quantities enables us to rewrite the equation of motion of the cosmic gas into a form that resembles its collisionless counterpart. The net force on the gas is then simply the gradient of an effective potential which can be computed from the density field alone.

The power of the method is enhanced by the fact that the density-temperature (or density-pressure) relation, which has to be input into the HPM computation, can be calculated for any reionization history in a very efficient manner without running hydrodynamic simulations (Hui & Gnedin 1997).

We have also shown that a somewhat worse accuracy (than that of HPM) can be achieved by a simple combination of a PM solver and smoothing of initial condition with an appropriate filter.

Both the PM + filtering method and HPM use a *single component* model to approximate what is in reality a *two-component* system. The HPM method, in particular, treats the dark matter as if it is subject to the same forces as the baryons, i.e. gravity as well as thermal pressure. As we have explained before, this should not be a problem on large scales, because pressure is dynamically subdominant on those scales anyway. On small scales, we are indeed introducing an error by allowing pressure to act on the dark matter: the dark matter distribution would become less clustered than it should be. One fact comes to our rescue, however: the dominant force on the baryons on small scales is thermal pressure, not gravity, and since pressure is determined by the baryon distribution alone, the actual distribution of baryons on small scales should not be sensitive to errors in the dark matter distribution. The good agreement between results of single-component HPM and full hydrodynamic simulations lends support to this interpretation.

We can perhaps understand this in a simpler setting. In Figure 2, the solid line shows the baryon fluctuation in the limit $f_b = 0$ (i.e. when no gravitational effect of the gas is included), while the dotted line marks the opposite case, $f_b = 1$, (when all the matter is treated as baryonic, or in other words, the dark matter is subjected to pressure similar to HPM). One might expect quite different behavior between the two cases, but in fact they are quite similar. Both on large scales and at very small scales (scales of oscillations), the fluctuations in both cases almost lie on top of each other. It is at the intermediate scales, in fact close to k_F, where the two depart from each other in a perceptible way. These scales

however span a rather small range, which is probably the reason behind the success of the single-component HPM.

Finally, a few words on the concept of maximum-likehood analysis of the Lyman-alpha forest observations. While the HPM method is a factor of 10-100 faster than the full hydrodynamic simulations, and only 25% slower than a single component PM simulation, it still requires considerable computational expense. One can imagine using a more efficient, but less accurate, approximation (say, truncated Zel'dovich approximation, see Hui et al. 1997) instead of HPM. This would introduce larger errors, but will allow us to sample a large parameter space of cosmological models. When a smaller set of plausible models is crudely identified with this technique, one can switch to the HPM and further narrow the allowed parameter space to a small region; finally, if higher accuracy is desired, several full hydrodynamic simulations can be run.

REFERENCES

Arons, J. 1972, ApJ, 172, 553

Bahcall, J. N., & Salpeter, E. E. 1965, ApJ, 142, 1677

Bertschinger, E. 1997, private communication

Bi, H. G., Borner, G., & Chu, Y. 1992, A&A, 266, 1

Bi, H. G., & Davidsen, A. F. 1997, ApJ, 479, 523

Black, J. H. 1981, MNRAS, 197, 553

Bond, J. R., Szalay, A. S., & Silk, J. 1988, ApJ, 324, 627

Cen, R. Y., Miralda-Escudé, J., Ostriker, J. P., & Rauch, M. R. 1994, ApJ, 437, L9

Coles, P., Melott, A. L., & Shandarin, S. F. 1993, MNRAS, 260, 765

D'Odorico, V., Cristiani, S., D'Odorico, S., Fontana, A., & Giallongo, E. 1997, A&A, in press

Doroshkevich, A. G. & Shandarin, S. 1977, MNRAS, 179, 95

Cristiani, S., D'Odorico, S., D'Odorico, V., Fontana, A., Giallongo, E., & Savaglio., S. 1996, MNRAS, in press (astro-ph 9610006)

Gnedin, N. Y. 1995, ApJS, 97, 231

Gnedin, N.Y. 1996, Ap.J, 456, 1

Gnedin, N. Y., & Bertschinger, E. 1996, ApJ, 470, 115

Gnedin, N. Y., & Hui, L. 1996, ApJ, 472, L73

Gnedin, N. Y., & Ostriker, J. P. 1999, ApJ, 486, in press (astro-ph 9612127)

Hernquist, L., Katz, N., Weinberg, D. H., & Miralda-Escudé, J. 1996, ApJ, 457, L51

Hu, E., Kim, T., Cowie, L. L., & Songaila, A. 1995, AJ, 110, 1526

Hui, L., & Gnedin, N. Y. 1997, MNRAS, accepted (astro-ph 9612232)

26

Hui, L., Gnedin, N. Y., & Zhang, Y. 1997, ApJ, 486, in press (astro-ph 9608157)

Ikeuchi, S. 1986, ApSS, 118, 509

Ikeuchi, S., & Ostriker, J. P. 1986, ApJ, 301, 522

Kirkman, D., & Tytler, D. 1997, ApJ, in press (astro-ph 9701209)

Kim, T., Hu, E. M., Cowie, L. L., & Songaila, A. 1997, AJ, in press (astro-ph 9704184)

Lu, L., Sargent, W. L. W., Womble, D. S., & Takada-Hidai, M. 1996, ApJ, 472, 509

McGill, C. 1990, MNRAS, 242, 544

Miralda-Escudé, J., Cen, R., Ostriker, J. P., & Rauch, M. 1996, ApJ, 471, 582

Mücket, J. P., Petitjean, P., Kates, R. E., & Riediger, R. 1996, A&A, 301, 417

Ostriker, J. P., & Ikeuchi, S. 1983, ApJ, 268, L63

Peebles, P. J. E. 1980, *The Large Scale Structure of the Universe*, Princeton: Princeton University Press

Petitjean, P., Mücket, J. P., & Kates, R. E. 1995, A&A, 295L, 9

Rauch, M., Miralda-Escud/'e, J., Sargent, W. L. W., Barlow, T., Weinberg, D. H., Hernquist L., Katz N., Cen R., & Ostriker
J. P. 1996, preprint, astro-ph 9612245

Rees, M. J. 1986, MNRAS, 218, 25

Rees, M. J. 1988, in QSO Absorption Lines, ed. J. C. Blades, D. A. Turnshek, & C. A. Norman (Cambridge: Cambridge Univ.
Press)

Wadsley, J. W., & Bond, J. R. 1996, to appear in Proc. 12th Kingston Conference, Halifax (astro-ph 9612148)

Weinberg, D. H., Miralda-Escudé, J., Hernquist, L., & Katz, N. 1997, ApJ, submitted (astro-ph 9701012)

Zhang, Y., Anninos, P., & Norman, M. L. 1995, ApJ, 453, L57

Zhang, Y., Anninos, P., Norman, M. L., & Meiksin, A. 1997, ApJ, in press (astro-ph 9609194)
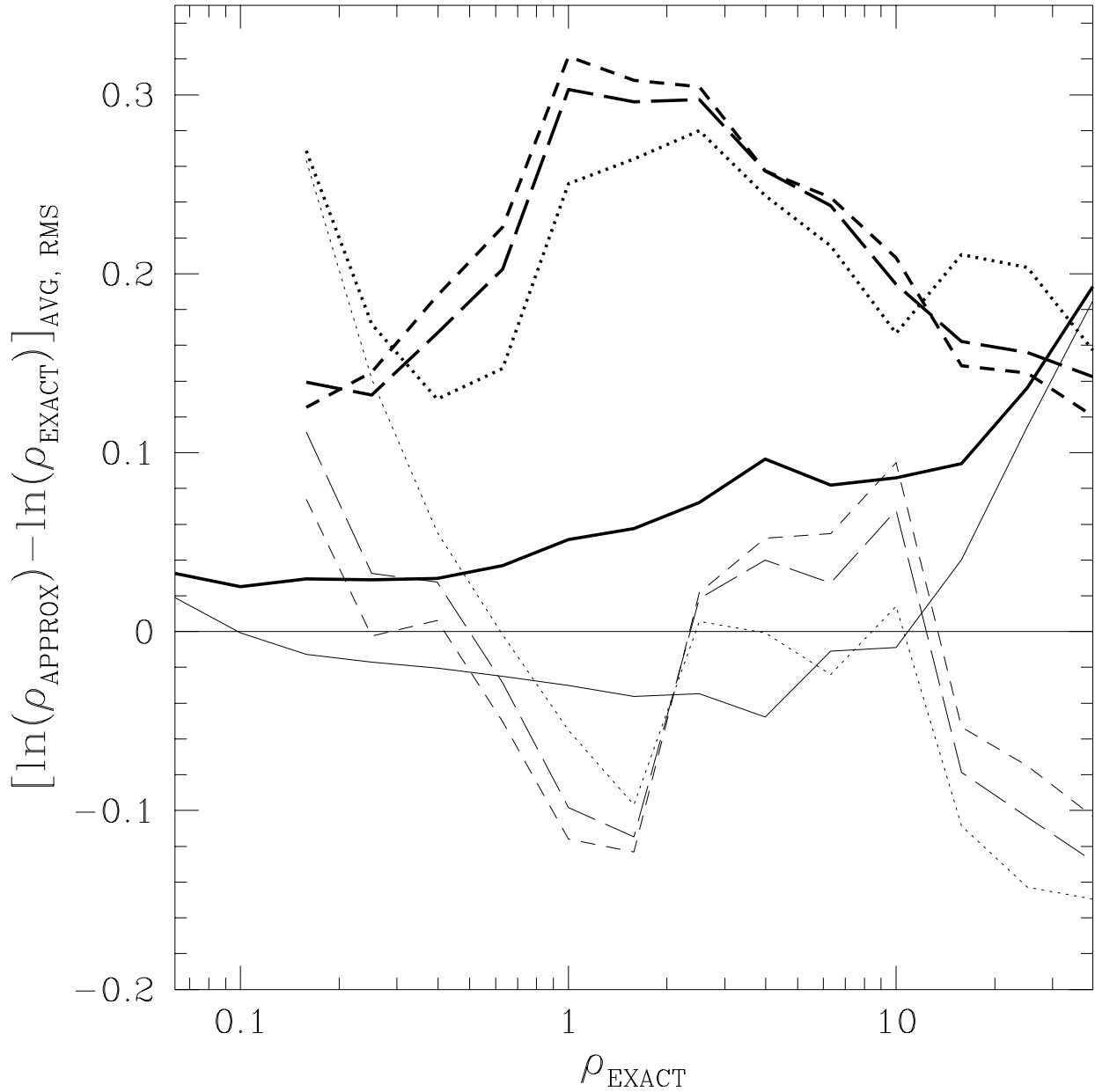
Figure 4. The average (*thin lines*) and rms (*bold lines*) fractional errors for the density fields in PM + filtering simulations as compared to the gas density field in a full hydrodynamic simulation for our SCDM model (see Table 1). The different approximations are: PM + $\exp(-k^2/k_F^2)$ smoothing (*dotted lines*), PM + $1/(1 + k^2/k_F^2)$ smoothing (*long-dashed lines*), and PM + best-fit smoothing (eq. 4.20; *short-dashed lines*). Also shown is a comparison between the dark matter density from the hydrodynamic simulation and the density from a PM simulation without any filtering (*solid lines*). The difference in the Green functions in the PM and hydrodynamic simulations induces an about 5% error.
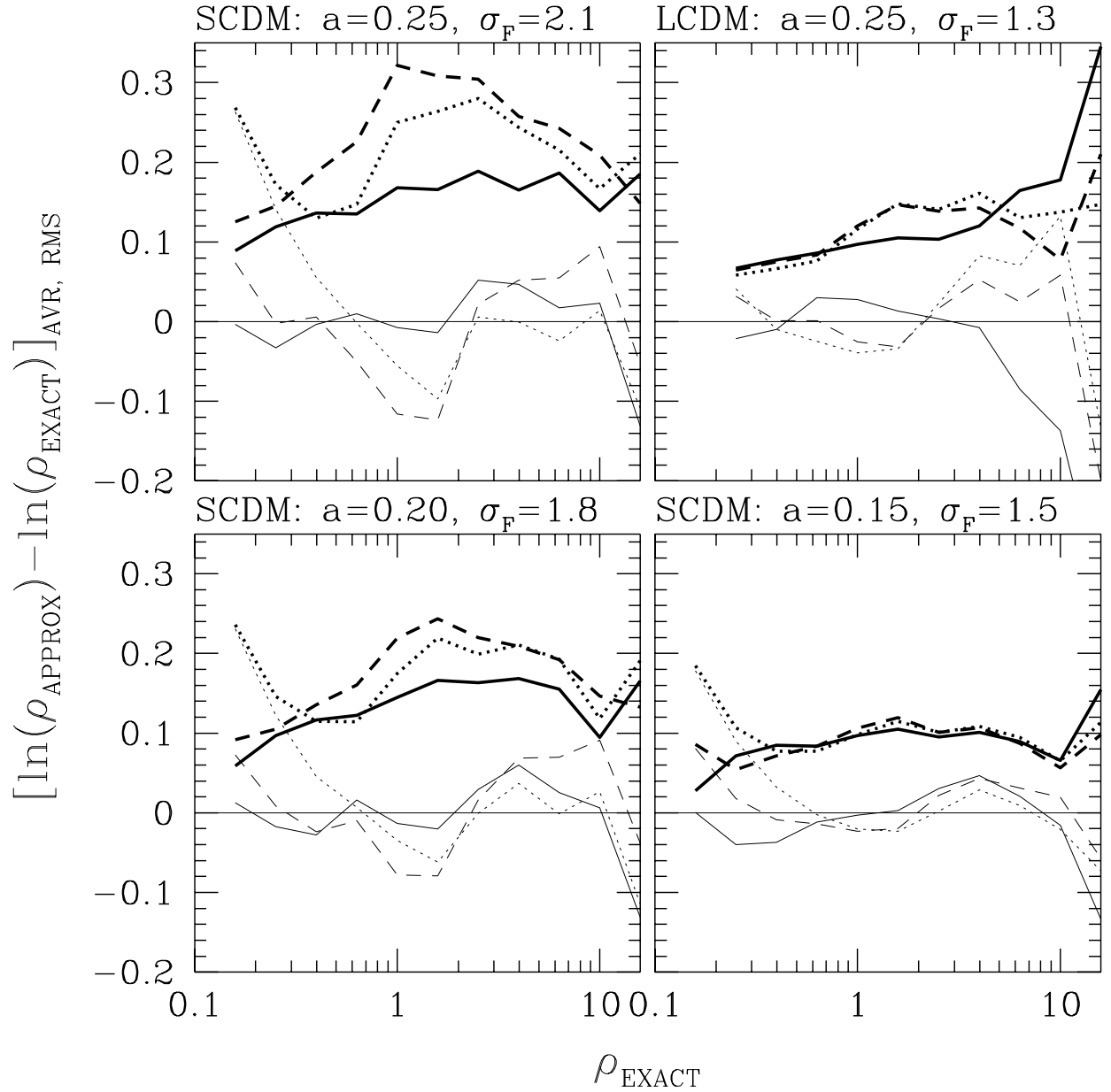
Figure 5. The average (*thin solid lines*) and rms (*bold solid lines*) fractional errors for the density fields in HPM simulations as compared to the gas density fields in full hydrodynamic simulations for SCDM and LCDM models, and for different stages of evolution, as labeled for each panel. For comparison, two variants of the PM + filtering method described in §3 are shown: PM + $\exp(-k^2/k_F^2)$ smoothing (*thin and bold dotted lines* for average and rms deviations compared with hydro) and PM + best-fit smoothing (*thin and bold dashed lines* for average and rms deviations compared with hydro) (see Fig. 4). The corresponding linear rms overdensity σ_F (eq. [5.25]) is also shown for each panel.
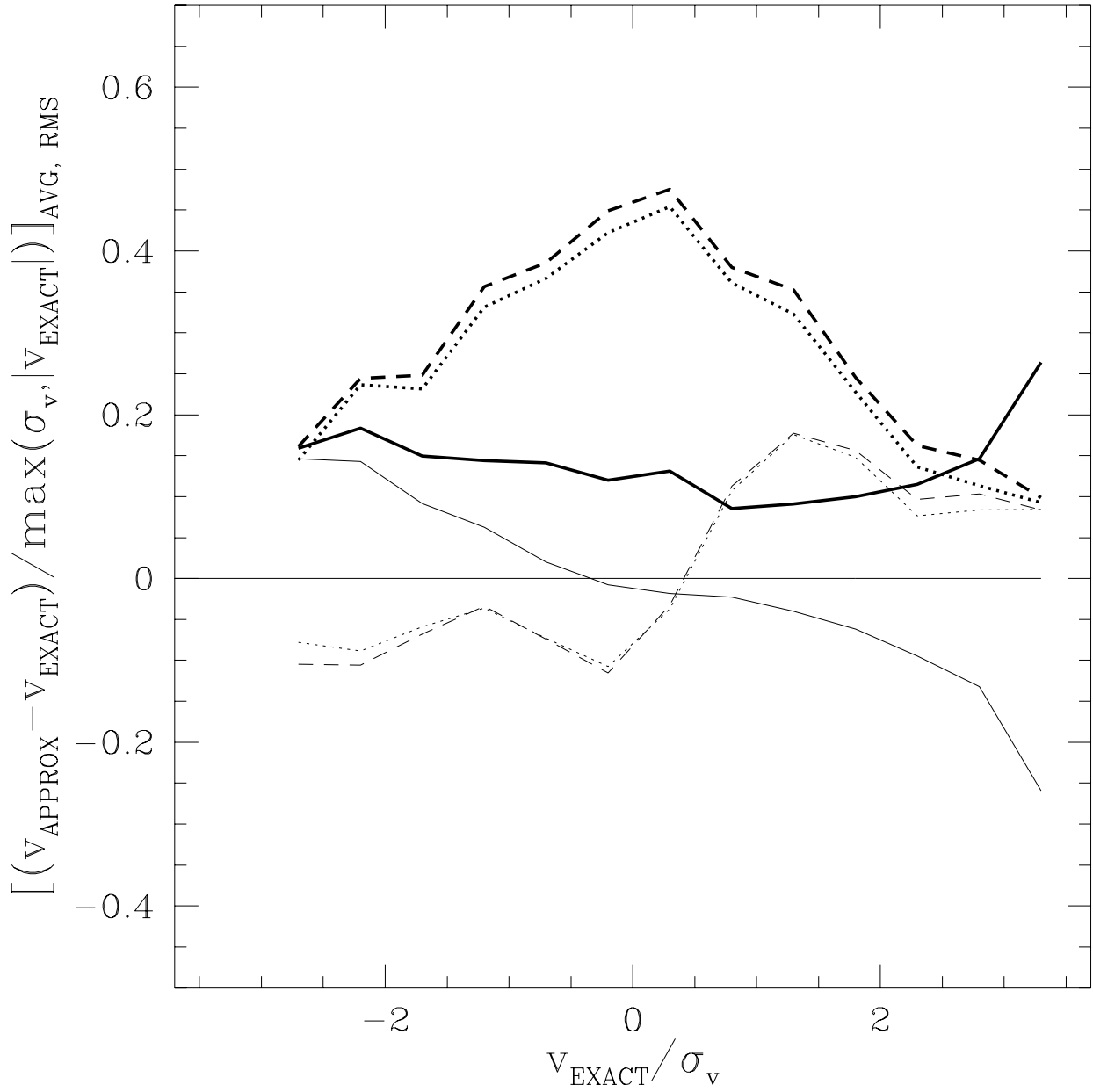
Figure 6. The average (*thin lines*) and rms (*bold lines*) fractional velocity errors for: HPM (*solid lines*), PM $+ \exp(-k^2/k_F^2)$ initial smoothing (*dotted lines*) and PM $+$ best-fit initial smoothing (eq. 4.20, *dashed lines*) as compared against the full hydrodynamic simulation for the SCDM model at $z = 3$.
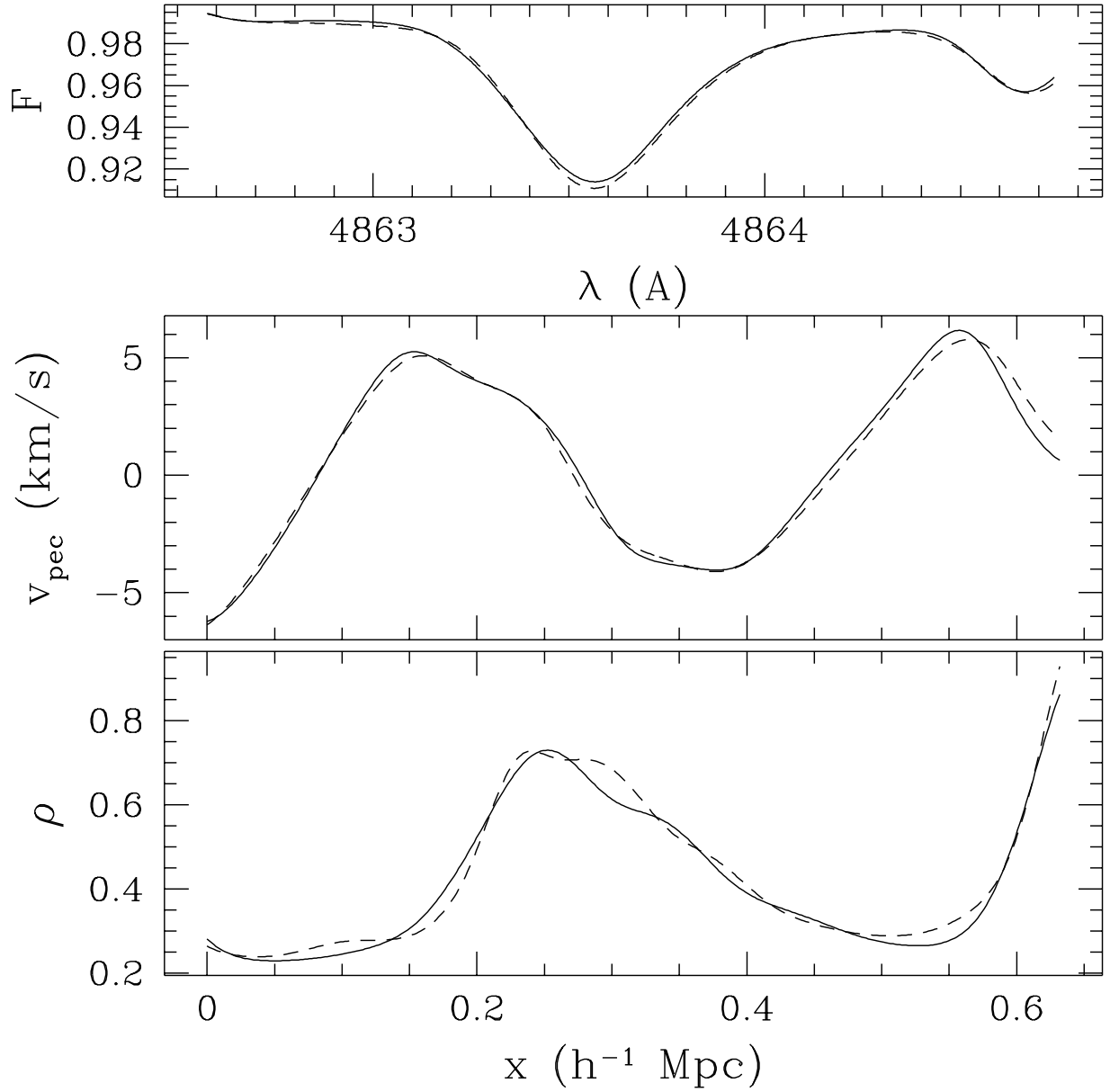
Figure 7. A line-of-sight comparison between a full hydrodynamic simulation (*solid line*) and the HPM (*dotted line*) for the SCDM model at $z = 3$. The bottom panel shows the density along the line-of-sight, the middle panel shows the peculiar velocity, and the upper panel shows the flux as a function of wavelength. This line-of-sight goes through an underdense region.
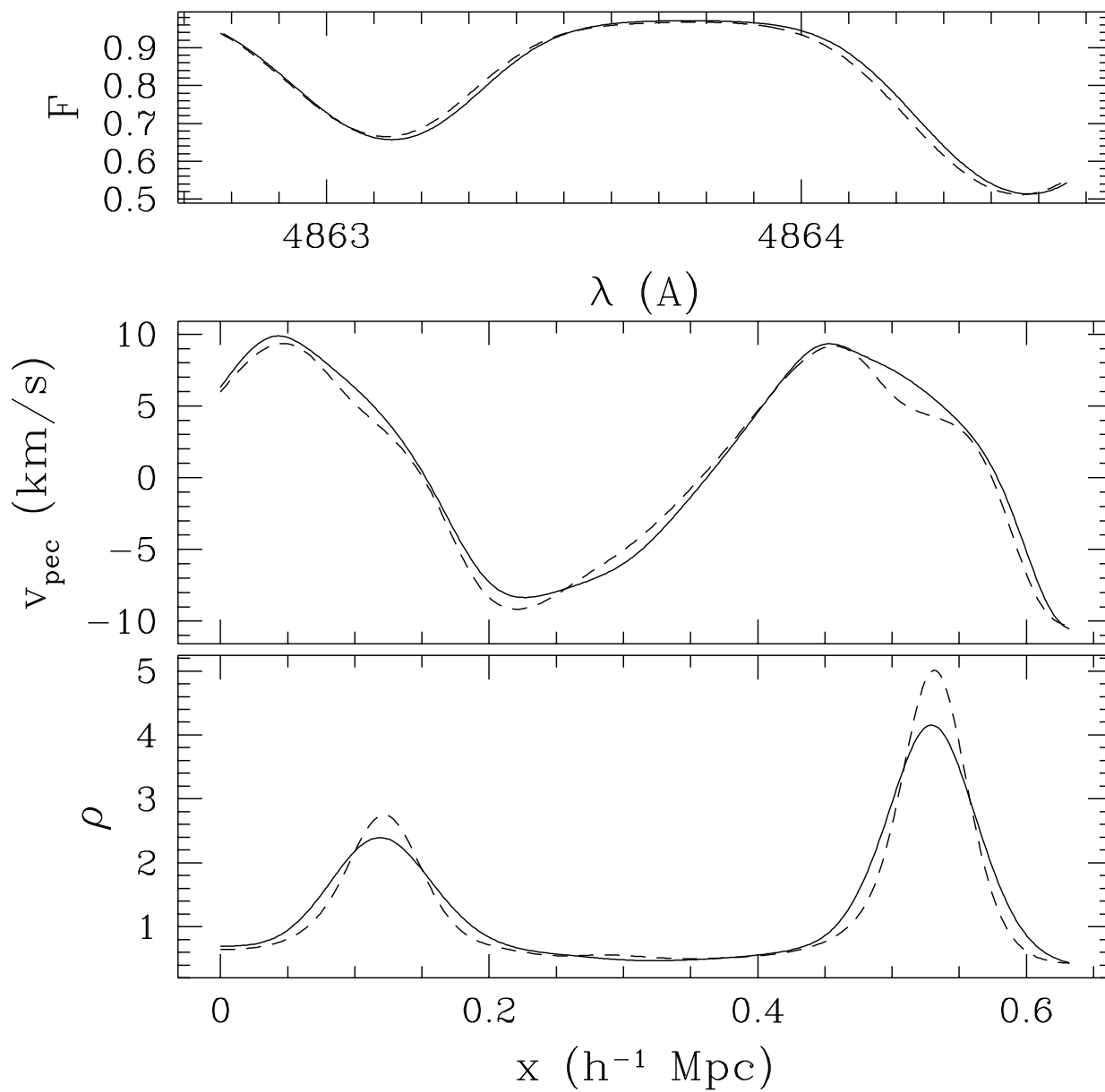
Figure 8. Another line-of-sight, which goes through an overdense region with $\delta < 10$.
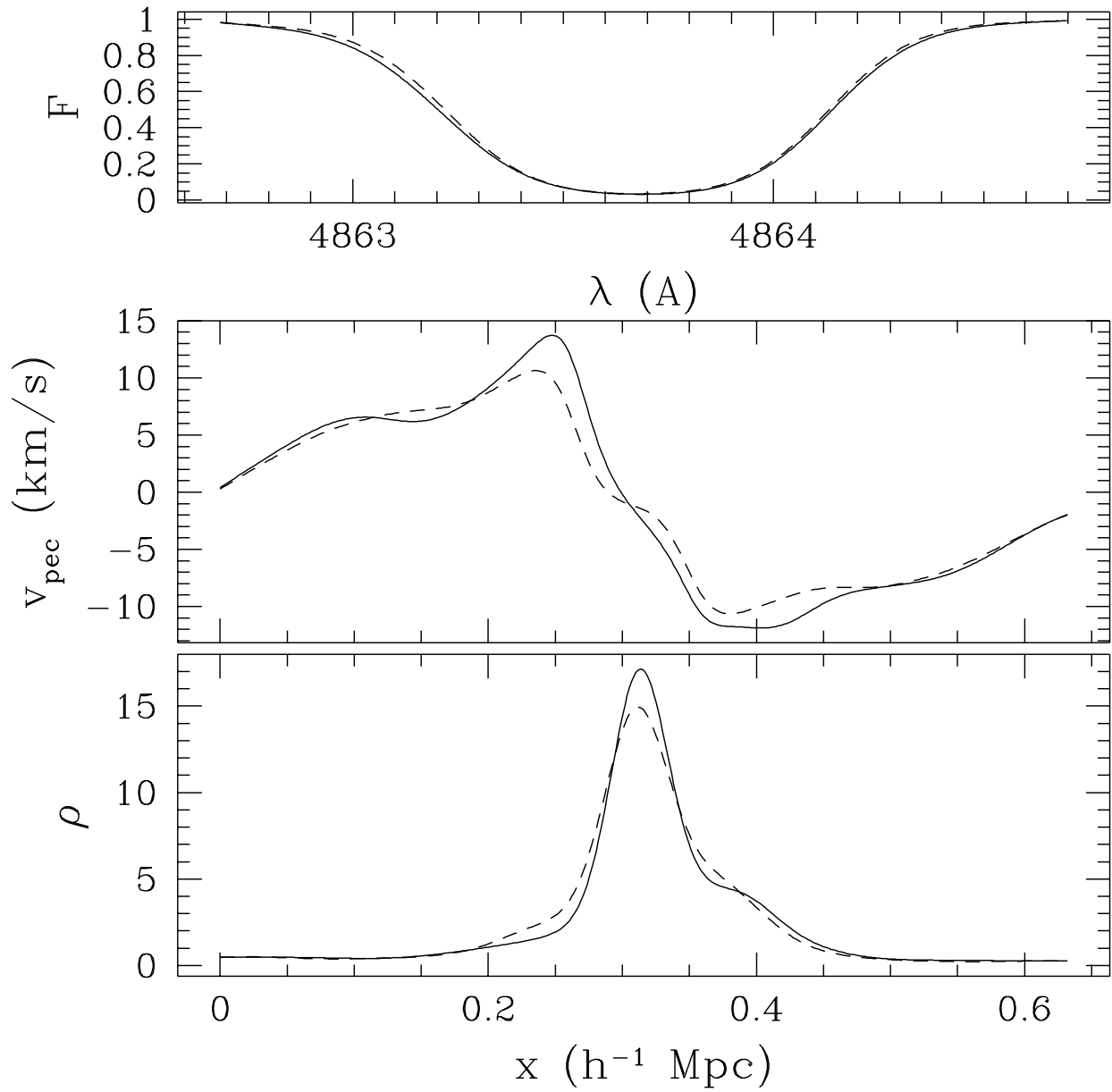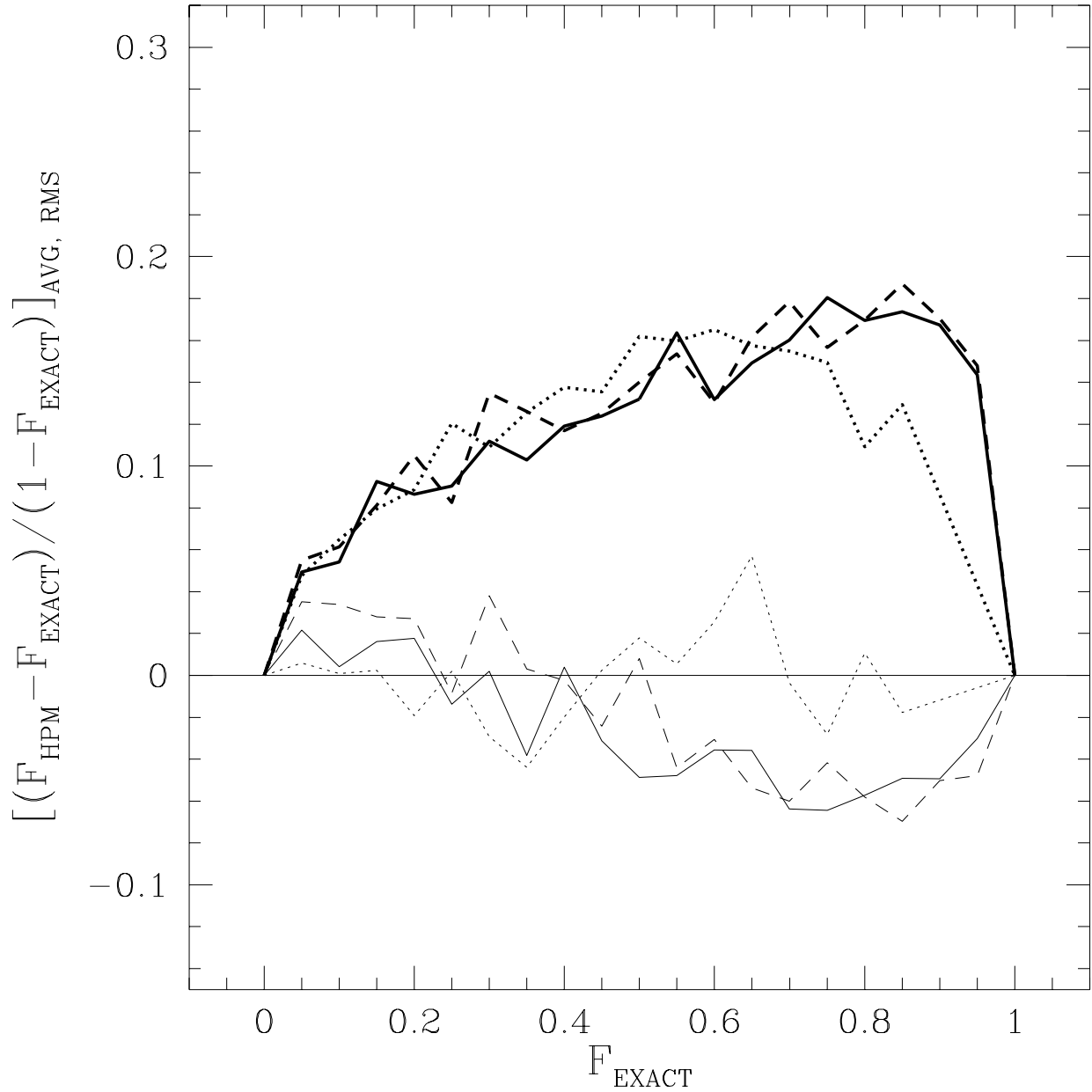
Figure 9. Another line-of-sight, which goes through a highly overdense region with $\delta > 10$. The HPM approximation is expected to break down in this regime.

Figure 10. The average (*thin lines*) and rms (*bold lines*) fractional decrement errors in an HPM simulation as compared to the full hydrodynamic simulations for the SCDM model at $z = 3$. The solid line shows the HPM versus the hydrodynamic simulation for $J_{21} = 0.3$, and the dashed line shows the same comparison for $J_{21} = 0.5$. Also shown is the case when the gas temperature is decreased by a factor of 100 to reduce thermal smoothing (*dotted line*) when generating the spectra.
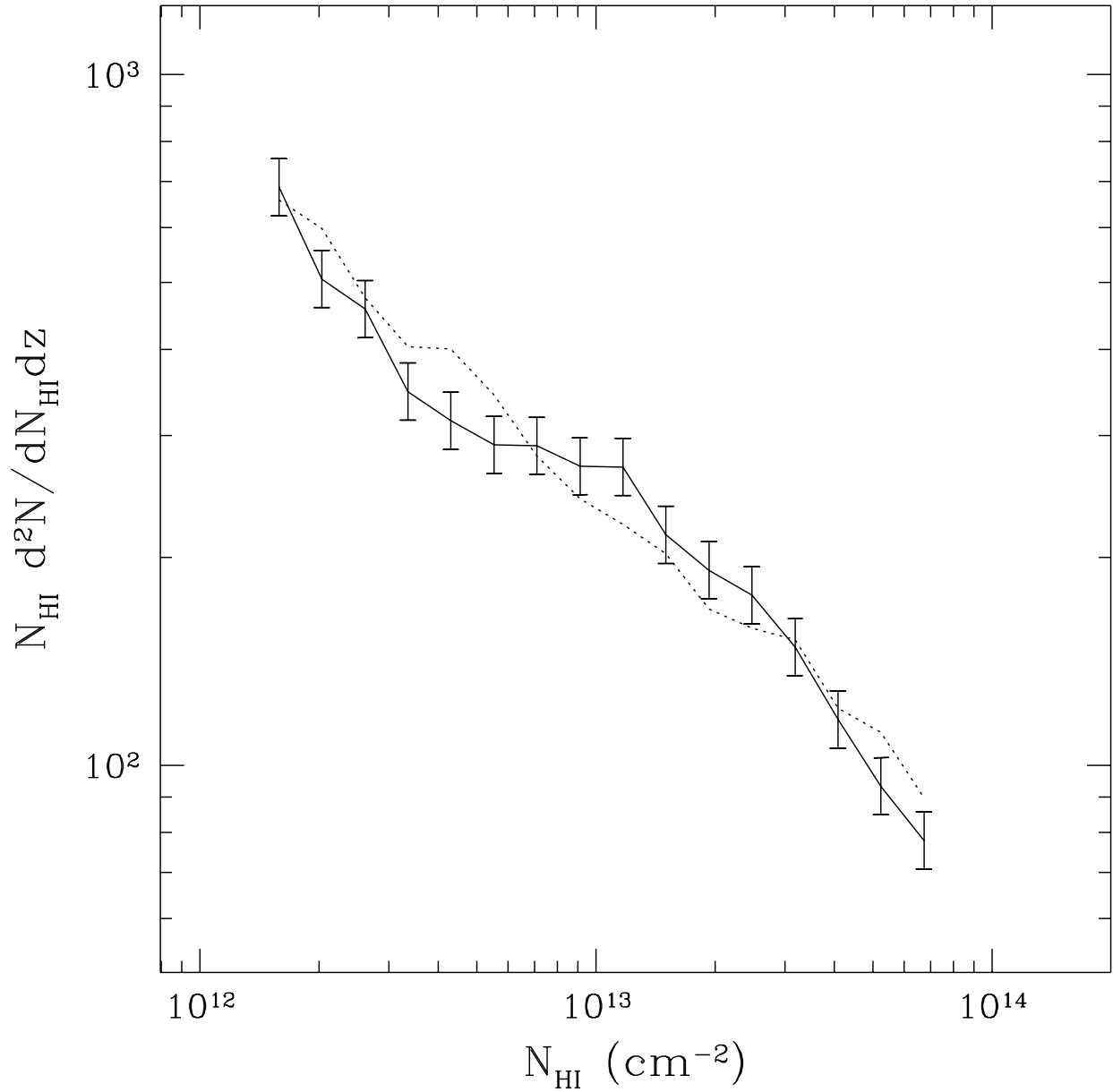
Figure 11. Column density distributions of the full hydrodynamic simulation (*solid line*) and the HPM approximation (*dotted line*) for the SCDM model at $z = 3$, computed using the Density-Peak Ansatz. A 10% error-bar was added for illustrative purpose only.